Applied Catalysis B: Environmental 129 (2013) 450–459

Contents lists available at SciVerse ScienceDirect

Applied Catalysis B: Environmental

journal homepage: www.elsevier.com/locate/apcatb

Transient studies of low-temperature dry reforming of methane over Ni-CaO/ZrO_2-La_2O_3

B. Bachiller-Baeza[a], C. Mateos-Pedrero[a], M.A. Soria[a], A. Guerrero-Ruiz[b], U. Rodemerck[c], I. Rodríguez-Ramos[a,*]

[a] Instituto de Catálisis y Petroleoquímica, CSIC, C/Marie Curie 2, Cantoblanco, 28049 Madrid, Spain
[b] Dpto. Química Inorgánica y Química Técnica, UNED, C/Senda del Rey 9, 28040 Madrid, Spain
[c] Leibniz-Institut für Katalyse e.V. an der Universität Rostock, Albert-Einstein-Str. 29a, 18059 Rostock, Germany

ARTICLE INFO

Article history:
Received 9 July 2012
Received in revised form
26 September 2012
Accepted 29 September 2012
Available online 8 October 2012

Keywords:
Dry reforming methane
TAP reactor
DRIFTS
Ni catalyst
Calcium oxide promoter

ABSTRACT

The low temperature reforming of methane by carbon dioxide is studied over a calcium oxide promoted Ni catalyst supported on a tetragonal zirconia stabilized by lanthana, which presents an improved stability compared to the non-promoted catalyst. Steady-state catalytic activity measurements, diffuse reflectance infrared Fourier transform spectroscopic analysis and isotopic temporal analysis of products experiments reveal the occurrence of a bifunctional mechanism on the promoted catalyst: methane is activated on the Ni particles, carbon dioxide interacts with the calcium oxide to form carbonates which scavenge carbon from nickel at the Ni-O-Ca interphase, thus restoring Ni particles to the original state. This is assumed to hinder the formation of deactivating coke, which explains the improved catalytic stability of the promoted catalyst. The main route for the carbon deposit formation is found to be the methane cracking in spite of the low temperature reaction.

1. Introduction

The reforming of methane by carbon dioxide has advantages over existing industrial processes for producing synthesis gas from both an environmental and an industrial perspective [1–3]. Thus, methane dry reforming could be beneficial to the environment since both CO_2 and CH_4 are greenhouse gases and this process provides a means to disposing them. From the industrial viewpoint, the reaction offers an alternative route for the production of syngas with a H_2/CO ratio close to one that can be used to tune the feed concentrations for the downstream reaction need.

Considerable efforts have been made to obtain catalysts for dry reforming to achieve both high activity and good stability [4]. Traditionally, nickel-based catalysts have been used for dry reforming of methane but they suffer from carbon deposition resulting in their rapid deactivation [5]. Most attempts aimed at improving activity and stability of Ni catalysts have been focused on synthesis conditions: using different types of supports and preparation methods, doping with alkaline or alkaline-earth metals etc. [6–11]. Dry reforming of methane is an endothermic reaction and thus high reaction temperatures are necessary to achieve high conversion degrees. Nevertheless, low temperature (<823 K) dry reforming of methane is an interesting approach to increase thermal efficiency and improve catalyst stability, as coke deposition by CH_4 decomposition is thermodynamically limited under these conditions. In addition the use of membrane reactors would lead to reach higher conversions by continuously extracting H_2 from the reaction zone [12,13].

Overall detailed understanding of the catalytic reforming process is required to develop high-performance catalysts for such reaction, that is, catalysts with a high activity and selectivity for the target products, CO and H_2, and with a low selectivity for coke formation. Although much effort has been spent on the investigation of the reforming mechanisms over the Ni-based catalysts at 873 K and above [14–17], to the best of our knowledge, the development of catalysts for reforming of methane is scarce for low temperature (673–823 K). However, it is known that the reaction temperature may remarkably affect the reforming mechanism [17].

In the work reported here, a Ni catalyst supported on lantana stabilized ZrO_2 and dopped with CaO is studied for the dry reforming of methane at 673–773 K. This catalyst was selected after screening an extensive variety of supported non-metal catalysts, using a wide range of different oxidic supports and promoters, for low temperature (673–823 K) methane reforming with CO_2 [18]. In order to further elucidate the role of the metal, of the promoter and of the support in the reaction cycle and to obtain key information on

* Corresponding author. Fax: +34 915854760.
E-mail address: irodriguez@icp.csic.es (I. Rodríguez-Ramos).

0926-3373/$ – see front matter © 2012 Elsevier B.V. All rights reserved.
http://dx.doi.org/10.1016/j.apcatb.2012.09.052

what makes these materials superior for reforming catalysts, temporal analysis of products (TAP) experiments were carried out at 723 K with different catalysts for the methane dry reforming. This fast transient kinetic method was found to apply perfectly to the mechanistic study of the various reactions dealing with methane activation [19,20]. For comparison purposes the non-promoted Ni/ZrO_2-La_2O_3 is also studied.

2. Experimental

2.1. Catalysts preparation and characterization

Commercial La_2O_3-ZrO_2 (MEL, SBET = 96 m^2/g) was used as support. Calcium oxide doped (2 wt%) zirconia was prepared by excess solution impregnation using a synthesis robot (Zinsser GmbH, Germany). Under vigorous shaking it was dosed 5.5 ml of aqueous calcium nitrate solution to the pre-shaped support (2 g, particle size 310–710 μm) followed by drying at 373 K for 2.5 h and calcining in static air at 923 K for 4 h resulting in 2 wt% Ca doped ZrLa support. The Ni-containing (ca. 5 wt%) catalysts were prepared by excess solution impregnation using the same synthesis robot. Under vigorous shaking 5.5 ml of aqueous nickel nitrate solution was dosed to the pre-shaped supports (2 g, particle size 310–710 μm), pure ZrLa or Ca doped ZrLa, followed by drying at 373 K for 2.5 h resulting in 5 wt% Ni loading ZrLa or Ca-ZrLa, respectively.

The nickel particle size, as determined from transmission electron microscopy measurements, for the ZrLa and Ca-ZrLa catalysts amounted to 2.9 ± 0.8 and 3.0 ± 0.7 nm, respectively. Over 200 individual metal particles were counted for each catalyst and the mean metal particle diameter (d_n) was calculated using the following equation.

$$d_n = \frac{\sum_i n_i d_i}{\sum_i n_i}$$

where n_i is the number of particles with diameter d_i.

2.2. In situ DRIFT spectroscopy

In situ diffuse reflectance infrared Fourier transform spectroscopy (DRIFTS) was applied to the study of the behavior of supported Ni catalysts, used in methane dry reforming, under various conditions. In situ DRIFT spectra were collected on a Varian 670 infrared spectrometer, with a Harrick Praying Mantis high-temperature cell with ZnSe windows, equipped with a liquid nitrogen cooled MCT detector. Spectra were obtained by collecting 200 scans with a resolution of 4 cm^{-1} and are presented in absorbance mode. The spectrum of an aluminium mirror was taken as background.

In one set of experiments, the interaction of a given gas (CO_2 or CH_4; CO_2 or CH_4/Ar = 2/16 ml min^{-1}) with both Ni-based catalysts was studied. In another case, the interaction of the same solid with the reaction mixture (dry reforming; CO_2/CH_4/Ar = 2/2/16 ml min^{-1}) was monitored at varying temperatures.

In all cases, the sample was loaded into the DRIFTS cell, then heated to 623 K under a flowing H_2/Ar mixture (H_2/Ar = 5/15 ml min^{-1}) and kept at this temperature for 2 h.

In a typical experiment, the sample was cooled to the desired temperature in flowing Ar, after which the solid was exposed to a flowing stream of CO_2/Ar or CH_4/Ar mixtures. In another experiment designed to analyze the formation of species during the dry reforming reaction, the reduced sample was contacted with the reaction mixture (CH_4/CO_2/Ar = 2/2/16).

The spectrum of the reduced sample after the reduction step was used as background. Finally, DRIFT spectra of the adsorbed species were obtained by subtraction of the spectrum corresponding to the reduced sample, from those obtained under CH_4/CO_2/Ar, CO_2/Ar and CH_4/Ar mixtures. The software provided by the manufacturer was used for data processing.

2.3. Steady state and transient experiments

Steady state experiments were carried out at atmospheric pressure in a fixed bed reactor. The reactor with an inner diameter of 9.3 mm was heated in an electric furnace equipped with a programmable temperature controller. 10 mg of fresh catalyst (particle size between 150 and 250 μm) was diluted with SiC to obtain 50 mm bed height and packed in the middle of the reactor. The temperature was monitored by a K-type thermocouple placed in the centre of the catalyst bed.

Before reaction the catalyst was reduced in situ at 773 K (maximum operation temperature) for 2 h with a mixture of 25 vol% H_2 in He at a flow of 100 ml/min. After reduction, He was used during 30 min to sweep H_2 from the reactor.

The feed gas mixture consisted of CH_4, CO_2 and He with a vol. percent ratio CH_4:CO_2:He = 10:10:80. The total flow rate was 100 ml/min (W/F = 1.7×10^{-6} g h/ml).

The lines before and after reactor were heated (at 383 K) to avoid water condensation. Prior to chromatographic analysis of the outlet reaction gases water was condensed employing a cool trap. Gas analyses of both reactants and products were carried out by on line GC (Varian 3400) equipped with a TCD detector.

The conversions (X), the yields (Y) and the H_2/CO ratio are calculated as follows:

$$X\mathrm{CH_4}(\%) = \frac{[\mathrm{CH_4}]_{in} - [\mathrm{CH_4}]_{out}}{[\mathrm{CH_4}]_{in}} 100$$

$$X\mathrm{CO_2}(\%) = \frac{[\mathrm{CO_2}]_{in} - [\mathrm{CO_2}]_{out}}{[\mathrm{CO_2}]_{in}} 100$$

$$Y\mathrm{H_2}(\%) = \frac{[\mathrm{H_2}]_{out}}{2 * [\mathrm{CH_4}]_{in}} 100$$

$$Y\mathrm{CO}(\%) = \frac{[\mathrm{CO}]_{out}}{[\mathrm{CH_4}]_{in} + [\mathrm{CO_2}]_{in}} 100$$

$$\frac{\mathrm{H_2}}{\mathrm{CO}}\mathrm{ratio} = \frac{\text{mol of } \mathrm{H_2} \text{ produced}}{\text{mol of CO produced}}$$

Preliminary experiments were performed at different loading and catalyst grain size to verify the absence of external and internal diffusion limitation. In addition, the inert properties of the supports in given conditions were checked. The carbon balance was close to 100% in all the cases.

All transient experiments were carried out in a TAP-2 reactor system which has been described in detail elsewhere [21]. Briefly, the apparatus consists of a catalytic micro-reactor, a gas delivery system for introduction of gas pulses or continuous flow of gas, a high vacuum system and a RGA-200 SRS quadrupole mass spectrometer. The microreactor was a stainless steel tube 0.38 cm in diameter and 2.54 cm long. The catalyst sample (50 mg, particle size 0.25–0.50 mm) was packed between two beds of silicon carbide (0.25–0.50 mm size) and the temperature measured by a thermocouple positioned in the center of the catalyst bed. Pulse intensities of $<10^{16}$ molecules were used to ensure Knudsen diffusion conditions, and Ar was used as internal standard for quantification of the results. Characteristic m/e ratios of reactants and products were followed: 40 (Ar), 44 ($^{12}CO_2$), 45 ($^{13}CO_2$), 15 ($^{12}CH_4$), 17 ($^{13}CH_4$), 28 (^{12}CO), 29 (^{13}CO), 2 (H_2) and 18 (H_2O). To increase the signal-to-noise ratio, from 15 to 20 pulses per atomic mass unit were averaged for the height-normalized responses. The CH_4 and CO_2 conversions were calculated using the reactant and the Ar peak areas. The CO and H_2 yields were based on the quantity of product

Table 1
Catalytic properties of nickel catalysts in reaction after 30 min at 723 K.

Catalyst	Ni-ZrLa	Ni-Ca-ZrLa
CH_4 conversion (%)	9.8 ± 0.5	9.1 ± 0.5
CO_2 conversion (%)	12.9 ± 0.6	12.0 ± 0.6
H_2 yield (%)	5.8 ± 0.3	6.1 ± 0.3
CO yield (%)	9.9 ± 0.5	9.2 ± 0.5
H_2/CO	0.58	0.67

detected. The maximum error in the conversions and yields was determined to be 5%.

Prior to the experiments the catalyst was reduced in a flow of H_2 at 773 K for 2 h, after which it was exposed to vacuum (10^{-9} Torr) at the same temperature. The following procedure was used for each catalyst:

- The dry reforming of methane was studied by means of vacuum pulse TAP experiments of the 1:1:1 CH_4/CO_2/Ar mixture.
- The same reaction mixture, CH_4/CO_2/Ar = 1/1/1, was pulsed over the sample after it was pretreated by injecting a series of successive pulses of two different mixtures: 2:1 CO_2/Ar mixture or 2:1 CH_4/Ar mixture.
- Finally, the reaction was carried out by pulsing a 1:1:1 $^{13}CH_4/CO_2$/Ar labelled mixture.

All the pulse sequences were carried out at 723 K.

Prior to each sequence of pulses, H_2 was pulsed over catalyst until the signal was stable to re-reduce the catalyst. Furthermore, at the end of the series of experiments the catalyst change was checked by repeating the first train of pulses, the 1:1:1 CH_4/CO_2/Ar mixture.

3. Results

3.1. Steady state catalytic testing

The catalytic activity of the Ni catalysts in the dry reforming of methane reaction was tested at 673, 723 and 773 K. Conversions of CH_4 and CO_2 and other reaction parameters, such as hydrogen yield, after 30 min at 723 K are shown in Table 1.

For the two catalysts, whatever the temperature, the conversion of CO_2 is higher than that of CH_4 (Table 1 and SI 1), suggesting that besides methane dry reforming, reverse water–gas shift reaction (RWGS) is also occurring. In general, CO_2 reforming of methane is typically accompanied by simultaneous occurrence of RWGS reaction [13,22]. In addition, whatever the temperature, *Y*CO is higher than *Y*H_2 for both catalysts (Table 1 and SI 2). This is in good agreement with that previously suggested, namely the RWGS also takes place because according to this reaction a part of the hydrogen produced by DRM is consumed producing CO from CO_2. Furthermore, the H_2/CO ratio (Table 1 and SI 3) is always less than 1.

Comparison of the two catalysts in the whole range of temperature studied reveals that they exhibit close CH_4 and CO_2 conversions. Additionally, Ni-ZrLa presents a higher *Y*CO (Table 1 and SI 2) and a lower H_2/CO ratio (Table 1 and SI 3) with respect to Ni-Ca-ZrLa. This indicates that the various reactions involved in the dry reforming of methane occur to different extent over the two catalysts as it will be discussed latter.

Fig. 1 shows the stability study conducted at 773 K for 14 h time on stream (TOS). It is observed that, although both catalysts deactivate, deactivation is much more drastic for Ni-ZrLa catalyst than for Ni-Ca-ZrLa.

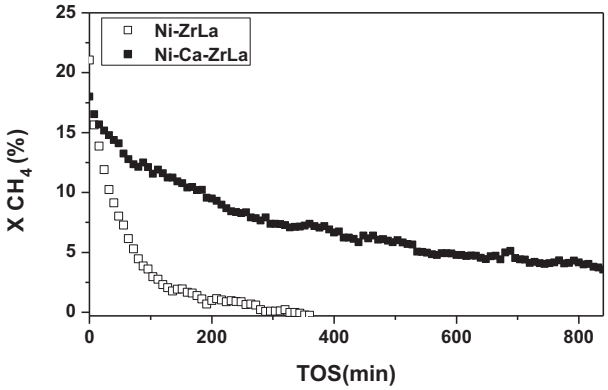

Fig. 1. Evolution of CH_4 conversion with time on stream at 773 K for Ni-ZrLa (□) and Ni- Ca-ZrLa (■).

3.2. DRIFTS

DRIFTS experiments were conducted under the reacting mixture CH_4/CO_2/Ar (2:2:16) at 773 K with the objective of identifying adsorbed intermediates species present under reaction conditions. Experiments were also performed in CH_4/Ar or CO_2/Ar in order to reveal the type of interaction between each reactant and the surface of the catalyst.

DRIFT spectra obtained under dry reforming conditions at 773 K for Ni-ZrLa and Ni-Ca-ZrLa samples (not shown for the sake of brevity) show as expected bands at 3016 and 1305, and 2360 and 2345 cm^{-1} which confirm the presence of gaseous CH_4 and CO_2 under reaction stream, respectively, for both catalysts [23–26]. In addition, two absorption bands corresponding to gaseous CO appeared at 2181 and 2121 cm^{-1} [27]. The presence of these bands resulted in poor resolution of the adsorbed species. After purging with Ar, small bands could be easily distinguished. Adsorbed CH_x species were not detected on the surface of the catalysts after Ar purge in dry reforming conditions. This phenomenon can be attributed to the fact that the surface reaction between adsorbed CH_x species and CO_2 (under dry reforming conditions) was relatively rapid. DRIFT spectra under dry reforming conditions after flushing with Ar over Ni-ZrLa and Ni-Ca-ZrLa at 773 K are displayed in Fig. 2. The spectra show a broad envelope between 1200 and 1700 cm^{-1} with distinct contributions, pointing to the presence of different carbonate species [28,29]. For the Ni-ZrLa sample the presence of monodentate carbonates species is evidenced by absorptions in the 1410–1520 cm^{-1} wavenumber range. Moreover, a shoulder centred around 1575 cm^{-1}, attributed to bidentate carbonates species, is easily distinguished in the spectrum of Ni-ZrLa. For the Ca-containing sample (Ni-Ca-ZrLa), the band is more symmetrical and two maxima centred at 1410 and 1515 cm^{-1} are clearly appreciated (Fig. 2A) corresponding to monodentate carbonate species. It is also observed that the concentration of species contributing to the band at 1575 cm^{-1} in the spectrum of the Ni-Ca-ZrLa would be lower compared with Ni-ZrLa. Therefore, it is interesting to find that a higher amount of monodentate surface carbonate species (1515 and 1410 cm^{-1}) were formed over the Ca-containing catalyst (Fig. 2A). The formation of these carbonate species can be ascribed to the reaction of CO_2 with surface oxygen species on the support which is enhanced by the presence of the basic promoter CaO [30–33]. At the same time, the carbonyl stretching mode of CO adsorbed on metallic surface characterized by several bands in the 1800–2100 cm^{-1} wavenumber region [34,35] could be detected for Ni-ZrLa and Ni-Ca-ZrLa. In Fig. 2B it is found that CO adsorbed linearly on reduced Ni sites (the most intense band at 2040 cm^{-1}) is

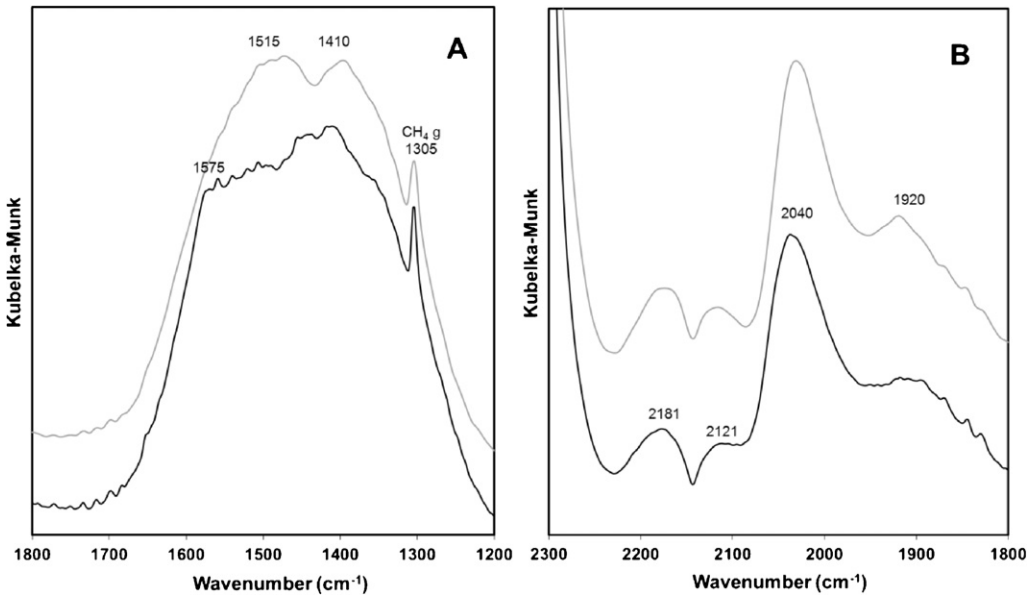

Fig. 2. Low wavenumber region DRIFT spectra obtained for Ni-ZLa (black line) and Ni-Ca-ZrLa (grey line) catalysts at 773 K under reforming conditions $CH_4/CO_2/Ar$ (2:2:16).

predominant. Another small band at around 1920 cm^{-1} evidences the appearance of bridge-bonded CO. Regarding the intensity of both bands, it is clear that linear CO species are predominant for both samples.

In the region of OH stretching frequencies (Fig. 3), a wide band around 3670 and a smaller band at 3730 cm^{-1}, better defined for the non-promoted sample, are observed for the fresh reduced catalysts. These bands can be assigned to hydroxyl groups on the support [31]. Under reaction conditions, an overall increase in intensity, more pronounced for the promoted sample, is observed in this region of the infrared spectrum, indicating the adsorption by the support of water molecules produced during the reaction. No clear evidences of other changes in OH bands exist due to the superimposed overtones of the CO_2 present in the gas phase in the region 3550–3700 cm^{-1}.

DRIFT spectra of the CH_4 adsorption after flushing with Ar over Ni-ZrLa and Ni-Ca-ZrLa at 773 K are displayed in Fig. 4A. Two broad bands centred at 2931 and 2860 cm^{-1} are appreciated after flushing with Ar for both catalysts (not shown). These bands are assigned to the asymmetric and symmetric stretching vibrations of CH_2 and CH_3 [23–26], and denotes the presence of adsorbed methane over the catalysts surface. Bands appearing in the 1600–2400 cm^{-1} region of the DRIFT spectra of Ni-Ca-ZrLa and Ni-ZrLa samples upon CH_4 adsorption evidence the presence of CO species (Fig. 4A). The sharp band at 2020 cm^{-1} observed in the spectra of both samples may be attributed to linear CO adsorption on reduced Ni sites [34,35]. As seen in Fig. 4A, the intensity of the band corresponding to linearly adsorbed CO species is higher for the Ca-containing sample, which suggests a higher concentration of these species on the surface of this sample in comparison with its Ni-ZrLa counterpart. The small bands below 2000 cm^{-1} (1780–1860 cm^{-1}) observed on both Ni-supported catalysts suggest the existence of bridged bonded CO species. These bands are characteristic of less dispersed Ni species. The bands observed above 2100 cm^{-1} (Fig. 4A) are present in both samples and might be ascribed to gaseous CO contribution. However, these bands above 2100 cm^{-1} are markedly different from those characteristic of gaseous CO and they can also be assigned to linear adsorbed CO species on cationic sites (either Zr^{4+} or Zr^{3+}), as reported for Pt/ZrO_2 catalysts elsewhere [36]. This adsorption involves the σ donation type to coordinatively unsaturated surface cationic sites, acting as Lewis acid centers, according to previous works [[36] and references hereafter].

In the spectra of CO_2 adsorption over both Ni-Ca-ZrLa and Ni-ZrLa solids at 773 K, gaseous CO_2 rotation-vibration P and R bands at 2360 and 2340 cm^{-1}, respectively, were detected. In addition, two small absorption bands corresponding to gaseous CO appeared at 2181 and 2121 cm^{-1}. After flushing with Ar, bands corresponding to CO species, linear (band at around 2030 cm^{-1}) and bridge (band centred at 1905 cm^{-1}), adsorbed on Ni sites were identified similar to those observed after CH_4 exposition (Fig. 4B). Moreover, on both catalysts several bands between 1600 and 1400 cm^{-1} became apparent, characteristic of carbonate type species adsorbed on the support at high temperature and similar to those formed under dry reforming conditions (Fig. 2A), the intensity of these bands being much higher for the Ni-Ca-ZrLa sample. The formation of CO under CO_2/Ar flow indicates the CO_2 dissociation on nickel sites.

3.3. Temporal analysis of products

3.3.1. Reaction mixture: CO_2–CH_4

Fig. 5 displays the conversion of CO_2 and CH_4, and the yields to CO and H_2 obtained from the integrated areas of the corresponding responses during a sequence of pulses of a CH_4–CO_2–Ar mixture for Ni-ZrLa (Fig. 5A) and Ni-Ca-ZrLa (Fig. 5B). Similar trends are observed for CH_4 and CO_2 conversions although with slightly higher values for Ni-Ca-ZrLa, 85 and 65% for CO_2 and CH_4 respectively, compared to those of the non-promoted catalyst, 75 and 58%, respectively. On the other hand, although the yields for CO and H_2 increase with increasing pulse number for both catalysts, Ni-Ca-ZrLa seems to reach stable values faster. Besides, while the production of H_2 is similar, the amount of CO produced on Ni-ZrLa catalyst is larger, 72% vs 38%, despite the lower consumption of CO_2. This great unbalance between the CO_2 consumed and the CO produced indicates that part of the reacted CO_2 on the Ni-Ca-ZrLa catalyst is retained in the form of carbonates, bidentate or monodentate, as already detected by DRIFTS.

The shape of the response curves obtained during the pulsing of the CH_4–CO_2–Ar mixture over the two catalysts is also different. The average responses for Ar, CH_4, CO_2, CO and H_2 in the first 15 pulses are displayed in Fig. 5C and D for Ni-ZrLa and Ni-Ca-ZrLa, respectively. Water signal is omitted due to the difficulty in the

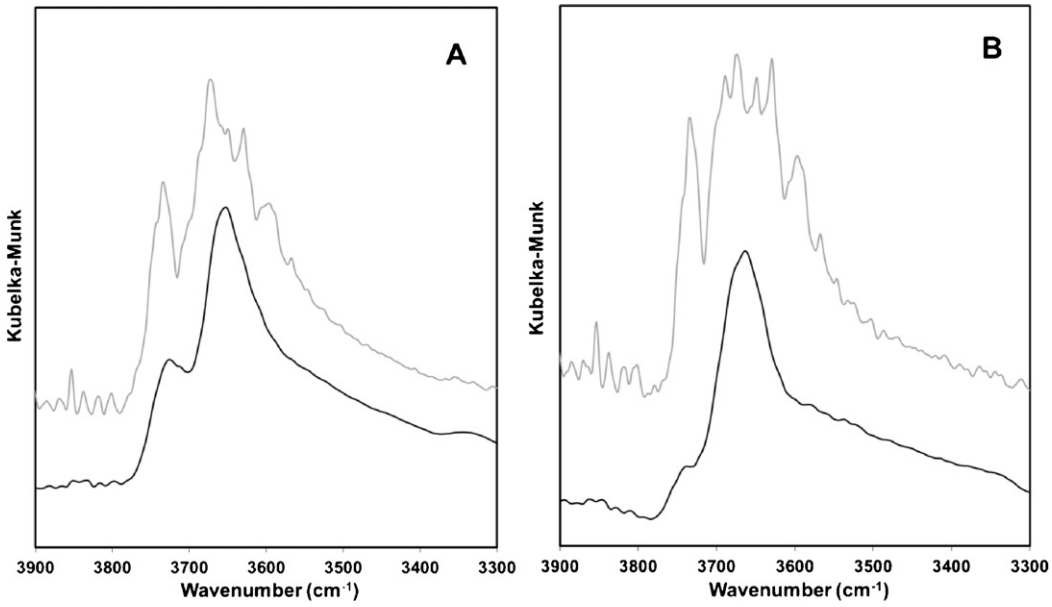

Fig. 3. OH stretching region DRIFT spectra of fresh reduced sample (black line) and after 30 min under reaction mixture (grey line) for Ni-ZrLa (A) and Ni-Ca-ZrLa (B) catalysts.

analysis of its transient. Since this study was conducted at 773 K it is very probably that desorption of water (if formed by RWGS) does not occur to a large extent. It is clearly revealed from these figures that CO_2, CO and H_2 peaks have longer tails for Ni-Ca-ZrLa catalyst suggesting stronger interactions of these compounds with the catalyst surface. Furthermore, H_2 curve seems to have two contributions, a fast and narrow H_2 response with peak times close to CH_4 peak time, and a second component, broader and with a longer tail, which is more significant for Ni-Ca-ZrLa.

3.3.2. *CH_4 and CO_2 pretreatment experiments*

The interaction of CH_4 and of CO_2 was measured over the reduced Ni-ZrLa and Ni-Ca-ZrLa by pulsing the individual gases, CH_4/Ar or CO_2/Ar, over both catalysts. Fig. 6A and C left side shows the CH_4 conversion and H_2 and CO production, calculated from the integrated areas of the response curves, as a function of the pulse number after a series of CH_4/Ar pulses for both catalysts. Although initial CH_4 conversions are similar, 60–70%, the evolution with pulse number was clearly different. The level of CH_4 conversion is maintained on Ni-Ca-ZrLa in contrast to Ni-ZrLa on which tends to fall completely. The amount of produced H_2 is initially small but gradually increases with increasing pulse number for both catalysts. Moreover, for the unpromoted catalyst H_2 production went through a maximum and then started to decrease slowly. This maximum roughly coincides with the point where CH_4 conversion also began abruptly to decrease. On the other hand, the H_2 yield seems to tend to a steady level for Ni-Ca-ZrLa. At the same time the production of CO was monitored for both catalysts, and again it seems to follow a different trend despite the similar initial values, around 25%. While for Ni-Ca-ZrLa the production of CO increases in the first 5 pulses for subsequently decreasing slowly, it drops to zero in the first 10 pulses for Ni-ZrLa. The average transient normalized CH_4,

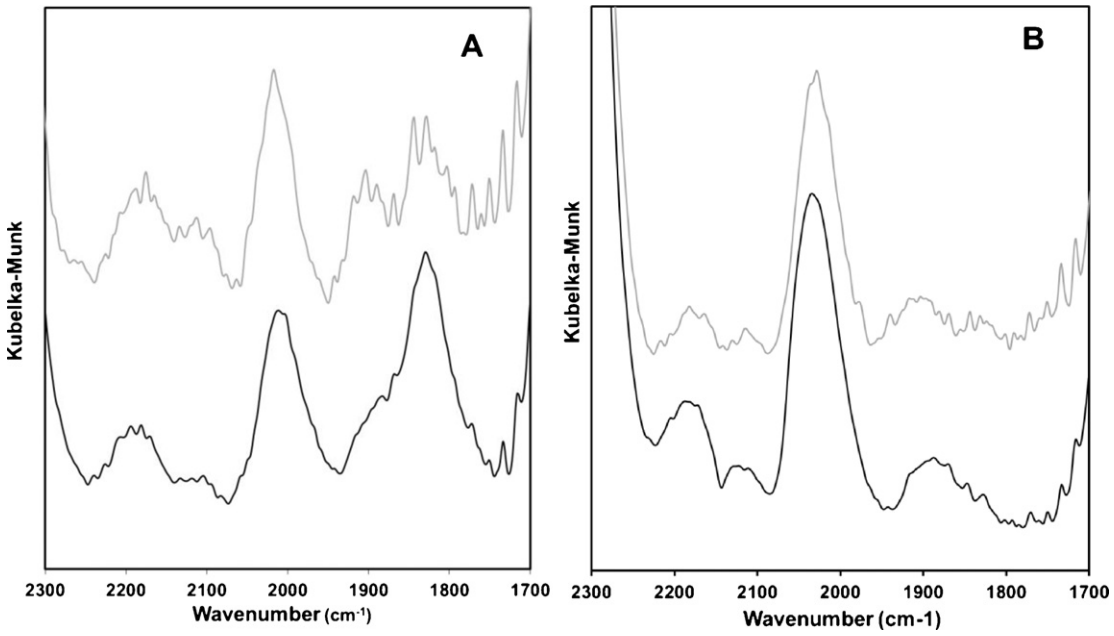

Fig. 4. DRIFT spectra of CH_4 (A) and CO_2 (B) adsorption over Ni-ZrLa (black line) and Ni-Ca-ZrLa (grey line) at 773 K.

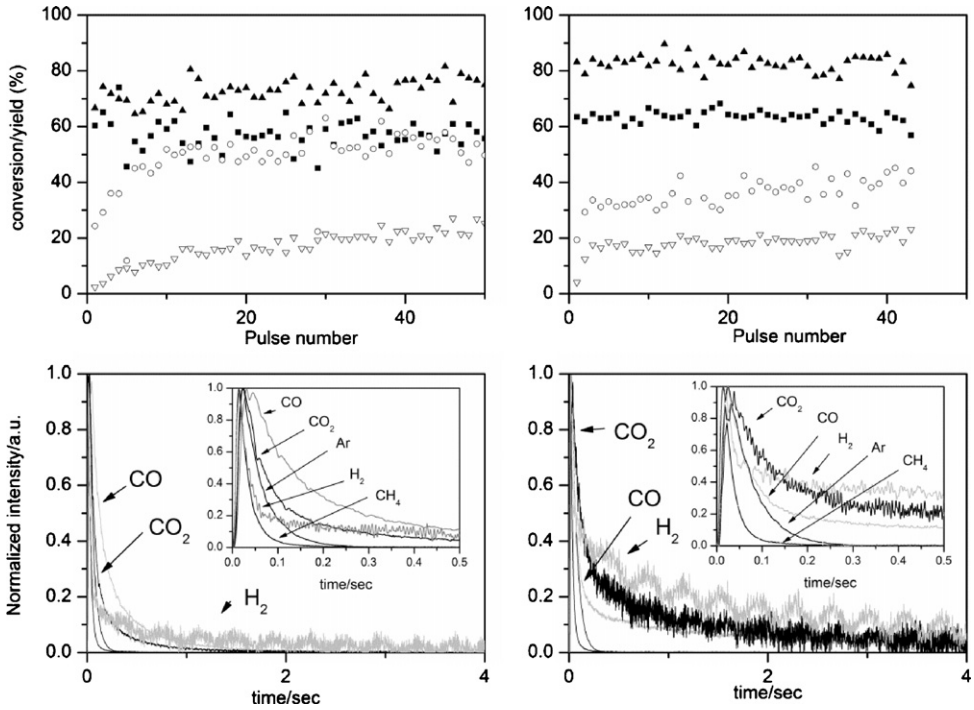

Fig. 5. CH_4 (■) and CO_2 (▲) conversion and H_2 (▽) and CO (◯) production vs pulse number obtained during CH_4–CO_2 multipulse experiment over reduced Ni-ZrLa (A) and Ni-Ca-ZrLa (B) catalysts at 773 K. Normalized responses of Ar, CH_4, CO_2, CO and H_2 during CH_4–CO_2 pulsing over Ni-ZrLa (C) and Ni-Ca-ZrLa (D).

H_2 and CO responses obtained for the first 20 pulses during this experiment for Ni-ZrLa and Ni-Ca-ZrLa samples were comparable (SI 4). Broad H_2 and CO response curves are observed probably as consequence of strong adsorption phenomena. Although, H_2 response gradually becomes narrower with increasing pulse number.

Pulsing of CO_2/Ar on Ni-ZrLa and Ni-Ca-ZrLa resulted in significant initial conversion values 90 and 85%, respectively (Fig. 6B and D, left side). Both CO_2 conversions are in the order of those obtained when $CH_4 + CO_2$ reaction was carried out (Fig. 5). The long tail of the CO_2 response suggests that part of the non-converted CO_2 is strong and reversibly adsorbed on the catalysts.

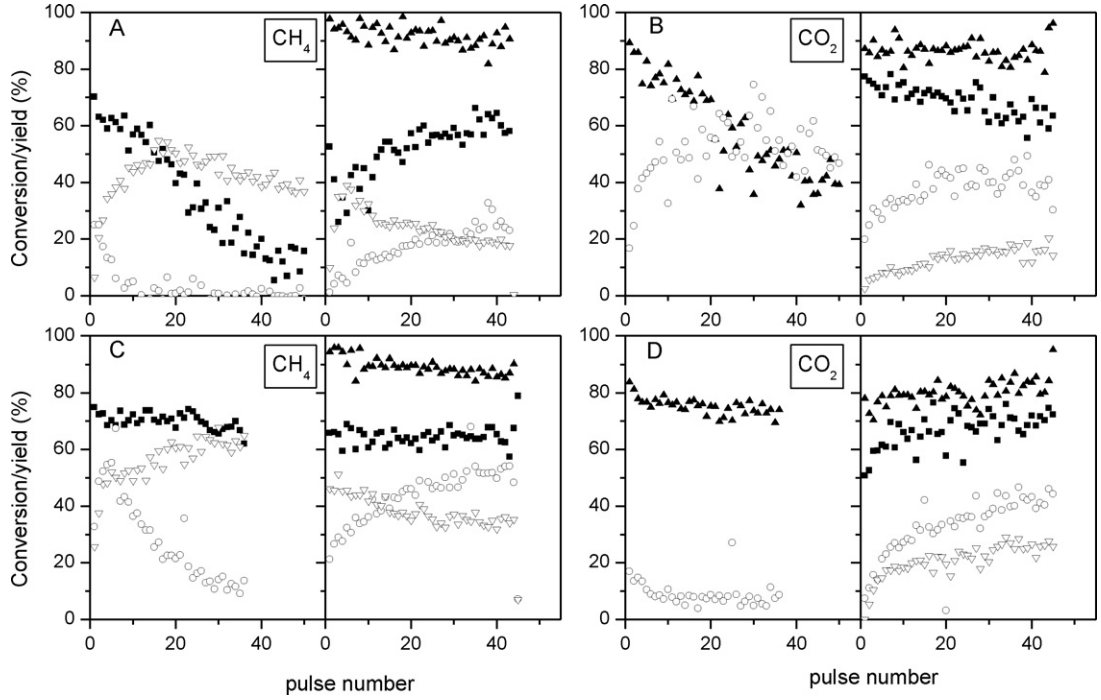

Fig. 6. CH_4 (■) and CO_2 (▲) conversion and H_2 (▽) and CO (◯) production vs pulse number over Ni-ZrLa (top) and Ni-Ca-ZrLa (bottom) catalysts at 773 K obtained during CH_4–CO_2 multipulse experiments (right side) after CH_4 (A and C) or CO_2 (B and D) pretreatments. The CH_4 (■) or CO_2 (▲) conversion and the H_2 (▽) and CO (◯) production during individual CH_4 or CO_2 multipulse experiments are shown on the left side.

However, this tail is significantly wide and pronounced for the Ni-Ca-ZrLa (shown in SI 4) indicating a much larger accumulation of CO_2 in this sample likely forming calcium carbonate, as already observed by DRIFTS (Section 3.2). Moreover, while conversions on Ni-ZrLa seems to decrease gradually with pulse number reaching a stable value of 40–50%, conversion values around 77% are maintained on Ni-Ca-ZrLa. Meanwhile the production of CO over Ni-ZrLa increases up to 50% (corresponding with the CO_2 conversion) after which it seems to be maintained. On the other hand, over Ni-Ca-ZrLa a low amount of CO (15%) is constantly formed far below the CO_2 converted. In any of the two catalysts although in a larger extent in the unpromoted catalyst, the reduced Ni is able to activate CO_2, retaining O abstracted from the CO_2 and supplying CO. In addition, the maintenance of the CO_2 conversion and the CO production along the pulsing experiment over the two catalysts suggests that Boudouard reaction which involves formation of carbon deposits, although thermodynamically favoured at the reaction temperature [22], is not significantly occurring.

After the above experiments, i.e. multipulse CH_4 or CO_2 pretreatment, the catalysts were probed with the reaction mixture CH_4–CO_2–Ar. The CO_2 and CH_4 conversions and the H_2 and CO yields as a function of the pulse number are displayed in Fig. 6(A–D right side) for Ni-ZrLa and Ni-Ca-ZrLa catalysts. CO_2 conversions higher than those obtained over the reduced catalyst (Fig. 5) were obtained for Ni-ZrLa after the CH_4 pretreatment, and CH_4 conversion increases from 25 to 60% with pulse number. CO production increases with pulse number leading at the end to level values of 23%, lower than that for the reduced sample. As far as the H_2 production is concerned, it follows a trend opposite to that for methane conversion, i.e. a maximum in the H_2 production, 40%, initially occurs after which the production decreases. The higher H_2 yield obtained in the first pulses can be likely due not only to the reaction product but also to H_2 still evolving after the CH_4 series of pulses. For the CO_2 pretreated Ni-ZrLa few differences with respect to the reduced catalyst are found. Thus, methane slowly decreases from 75 to 65% and the values for CO production increase with pulse number, and although higher than those for the CH_4 pretreated sample they are still lower than those obtained over the reduced surface. The production of H_2 is similar to that for the reduced catalyst and also increases with pulse number from very low levels up to 18%.

A different behaviour is observed for Ni-Ca-ZrLa. Compared to the reduced catalyst, pretreatment with CH_4 results in slightly higher initial CO_2 conversion, that slowly decreases with pulse number, and similar CH_4 conversion. On the other hand, while CO production constantly increases reaching higher values, H_2 yield decreases from 50 to 35%. This trend is similar to that observed for the unpromoted Ni-ZrLa catalyst. After CO_2 pretreatment, both CH_4 and CO_2 conversions increase with pulse number. The amounts of H_2 and CO initially produced are very small but gradually increase to values similar to those obtained for the reduced catalyst.

Comparison of the shape of CO and H_2 response curves recorded at the initial stages and at the end of the experiment when the reaction mixture is pulsed over the CH_4 or CO_2 pretreated surface reveals changes as a function of the pulse sequence, especially for the H_2 response (shown in SI 5). For Ni-ZrLa, while the shape for CO and H_2 responses slightly changes after the CO_2 pretreatment, some differences can be observed in their profiles for the CH_4 pretreated surface. CO is narrower than for a fresh surface and the H_2 peak is transformed with pulse number from an initially wide peak to a narrower peak with longer tail similar to that obtained over the reduced surface.

For Ni-Ca-ZrLa, CO response became wider with increasing pulse number in all three cases: reaction over reduced surface, over CH_4 pretreated surface or CO_2 pretreated surface. Also the tail or second slower peak in the H_2 curve increases with pulse number or time for all the surface states, but particularly for the CH_4 pretreated surface where in the initial stages H_2 seems a wide peak as it was observed for Ni-ZrLa sample pretreated with CH_4.

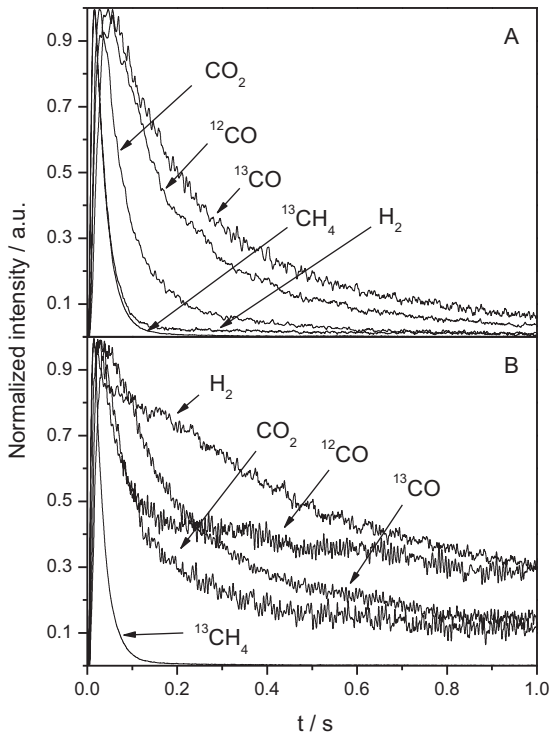

Fig. 7. Normalized responses of CO_2, ^{13}CO, ^{12}CO and H_2 during $^{13}CH_4$–CO_2 pulsing over Ni-ZrLa (A) and Ni-Ca-ZrLa (B).

3.3.3. *Isotopic reaction mixture: $^{13}CH_4$–CO_2*

The responses for Ar, $^{13}CH_4$, $^{12}CO_2$, ^{13}CO, ^{12}CO and H_2 were monitored during the pulsing of the $^{13}CH_4$–$^{12}CO_2$ mixture over reduced Ni-ZrLa and Ni-Ca-ZrLa catalysts, and Fig. 7 displays the average normalized responses for the 20 last pulses for $^{12}CO_2$, ^{13}CO, ^{12}CO and H_2. No signal ascribed to $^{13}CO_2$ was obtained. The $^{13}CH_4$, CO_2 and H_2 response curves obtained for both catalysts are similar to those obtained after the pulse of the unlabelled mixture. For Ni-Ca-ZrLa, CO_2 presents a longer tail which again indicates some kind of interaction of this compound with the support. And, while H_2 response for Ni-ZrLa is a narrow peak with a long tail, for Ni-Ca-ZrLa the peak is very wide, with a pronounced tail and can be deconvoluted into two contributions as indicated above, a first narrow due to fast desorption and a second slower desorption peak. The wide responses for ^{12}CO and ^{13}CO with some tailing are similar in shape for Ni-ZrLa although ^{13}CO is slightly delayed. However, the shapes of the ^{12}CO and ^{13}CO responses obtained over Ni-Ca-ZrLa are distinct. ^{13}CO is also broad and delayed with respect to ^{12}CO, and its maximum peak time (t_p) is similar to that for the non-promoted sample. On the other hand, ^{12}CO seems to present two contributions, a first fast desorption with a lower t_p than for Ni-ZrLa, and a second with a longer residence time in the same way as it is also observed for H_2. Although it is not shown, for the Ni-Ca-ZrLa sample the H_2 peak progresses with pulse number as indicated above for the pulses of the non-labelled mixture, i.e. the second contribution became dominant. However, the profile for ^{12}CO does not depend on the pulse number and remains constant while ^{13}CO tends to be broader which would explain the results observed with the non-labelled mixture.

The $^{12}CO/^{13}CO$ ratio determined from the non-normalized peaks was around 2 for Ni-ZrLa and 1.2 for Ni-Ca-ZrLa, and variation was not detected all along the pulsing experiments.

4. Discussion

All the results reported above show a strong influence of the promoter on the catalytic behaviour, clearly indicating changes in the reaction mechanism depending on the catalyst. We will present an interpretation of the results in term of reaction mechanism for the two catalysts comparatively. The main features demonstrated in the present study are the following:

1. *Individual methane pulsing:*

CO and H_2 were formed after the methane pulsing over both of the fresh reduced catalysts. This indicates that dissociation of the CH_4 occurred on the Ni crystallites during the methane pulse, as described for studies at higher temperatures [15,37], producing surface carbon species that then react rapidly with oxygen species to produce CO (as supported by DRIFTS and TAP experiments). This latter is effective and continuously produced on the CaO promoted catalyst which possesses plenty of oxygen species at the interfacial area between Ni nanoparticles and the promoter. On the non-promoted catalyst the oxidation of the carbon species on the Ni particles involves the participation of oxygen species (likely hydroxyl groups) in the interfacial area of the Zr-La support. The CH_4 conversion and CO production on the non-promoted catalyst rapidly decay indicating that once the most of the available surface oxygen is consumed the carbon species produced by CH_4 decomposition remain on the surface of the Ni nanoparticles forming deactivating coke which would hinder the subsequent CO_2 activation. Participation of the oxygen of zirconia support has been reported during dry reforming of methane over Rh/ZrO_2 [20,38], Ni-CaO-ZrO_2 [11] and Pt/ZrO_2 [39]. In addition, in the latter TAP study [39] it was also suggested that participation of zirconia oxygen species is only restricted to the surface which is in agreement with our results.

2. *Individual carbon dioxide pulsing:*

CO was produced upon CO_2 pulsing on the fresh catalysts by dissociation on Ni nanoparticles leaving oxygen on the metallic surface as it has already been reported in the literature [19]. The CO formation was recognized by DRIFTS and also assessed by TAP experiments. On Ni-ZrLa the CO formation approaches the stoichiometric amount after 10 pulses. The deficiency in the carbon mass balance upon CO_2 pulsing on Ni-Ca-ZrLa over the whole range indicates that not only CO_2 dissociation but also a continuous CO_2 storage in the form of carbonates takes place on the CaO promoter. The formation of calcium carbonate (expected given the strong basicity of the CaO) is supported by the higher amount of surface carbonate species shown in DRIFT spectra of Ca containing catalyst. Moreover, the long tail of CO response peak supports the reversible decomposition of the carbonates. No appreciable deactivation of the catalysts upon CO_2 pulsing was observed. Therefore, carbon formation on the nickel particles by CO disproportionation reaction is not occurring.

3. *Reaction mixture: CO_2–CH_4:*

The CH_4–CO_2 reaction over Ni-ZrLa and over Ni-Ca-ZrLa produces very low yields of H_2 what indicates, as supported by the DRIFT spectra, that it is probably oxidized and stored on the support in the form of hydroxyl groups as intermediates to water. Very low hydrogen yields in high temperature dry reforming of methane were also reported during TAP experiments over Pt/Al_2O_3 [39]. This reaction would be part of the reverse water-gas shift equilibrium, generally achieved under high temperature reforming conditions [19]. The second slow contribution observed on the H_2 response, more prominent for Ni-Ca-ZrLa, could be due to the reverse spillover of the support hydroxyl species, and its broadening and increment with pulse number could be due to a higher hydration or hydroxylation grade as the reaction progresses. Thus, the rate of H_2 desorption is limited by the migration and diffusion of these hydroxyl species from the support to the metal particles. The lower H_2/CO ratio for Ni-ZrLa compared to that for Ni-Ca-ZrLa could be due to the storage of CO in the form of calcium carbonates on the latter catalyst. CH_4 or CO_2 pretreatments do not affect the CH_4–CO_2 reaction on the promoted sample. However, on the unpromoted sample the CH_4 pretreatment leads to decreased methane conversion during the first 10–20 group of pulses due to the carbon deposits previously accumulated.

$$CH_4 + 5Ni \rightarrow NiC + 4Ni\text{-}H \quad [1]$$

$$CO_2 + 2Ni \rightarrow Ni\text{-}CO + NiO \quad [2]$$

$$NiO + Ni\text{-}H \rightarrow Ni + Ni\text{-}OH \quad [3]$$

$$NiC + Ni\text{-}OH \rightarrow Ni\text{-}CO + Ni\text{-}H \quad [4]$$

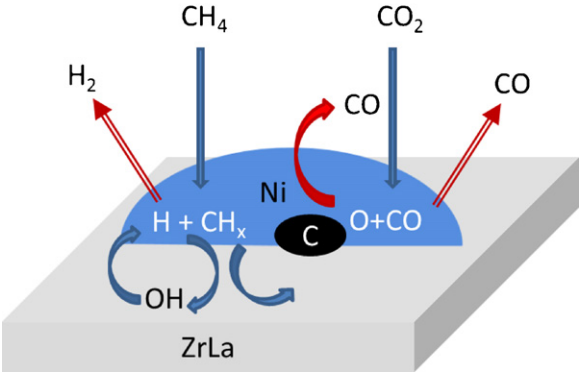

Fig. 8. Scheme and reaction steps for the low temperature dry reforming of methane over Ni-ZrLa catalyst.

4. *Isotopic reaction mixture: $^{13}CH_4$–CO_2:*

The $^{13}CH_4$–CO_2 experiments reveal that CO and ^{13}CO are produced along the pulses and their shapes and relative intensities are different over the two catalysts. The $CO/^{13}CO$ ratio was higher on Ni-ZrLa (around 2) than on Ni-Ca-ZrLa (around 1.2) which supports the accumulation of carbon deposits arising from methane cracking on nickel metal in the former catalyst. Moreover, the long tailing of the unlabelled CO on the promoted catalyst simply derived from the carbonate decomposition accumulated on the promoter.

To account for the above exposed features, two different reaction mechanisms are proposed for the low temperature (673–773 K) methane reforming with carbon dioxide for each of the nickel catalysts, which describe their different behaviour in reaction of each and involve their resistance to carbon deposition. Schemes in Figs. 8 and 9 summarise the elementary steps for Ni-ZrLa and Ni-Ca-ZrLa, respectively.

For the case of Ni-ZrLa (Fig. 8), both CH_4 and CO_2 activations are assumed to occur directly on the metallic surface (steps 1 and 2). Step 3 accounts for the low yield of hydrogen which is probably spilled over and stored on the Zr-La surface in the form of hydroxyl groups. Reverse spillover of hydroxyl groups from support onto nickel particles provide the oxygen species necessary for step 4. Carbon dioxide dissociation over nickel (step 2) can be considered a slower step than methane cracking (step 1) therefore this latter conduces to carbon deposition and catalyst deactivation once the oxygen on the nickel surface is consumed. Indeed, the

$$CH_4 + 5Ni \rightarrow NiC + 4Ni\text{-}H \quad [1]$$

$$CO_2 + CaO \rightarrow CaCO_3 \quad [2]$$

$$CaCO_3 + (Ca\text{-}ZrLa)\text{-}H \rightarrow CO + (Ca\text{-}ZrLa)\text{-}OH + CaO \quad [3]$$

$$NiC + (Ca\text{-}ZrLa)\text{-}OH \rightarrow Ni + CO + Ca\text{-}ZrLa + H \quad [4]$$

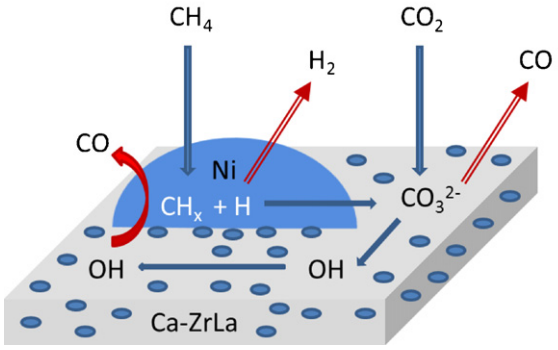

Fig. 9. Scheme and reaction steps for the low temperature dry reforming of methane over Ni-Ca-ZrLa catalyst.

experiment with the isotopic reaction mixture ($^{13}CH_4$–CO_2) shows that the ^{13}CO response derived from methane is much smaller than that of CO indicating that large accumulation of carbon (^{13}CO precursor) is occurring.

Such mechanistic scheme does not apply anymore for Ni-Ca-ZrLa because the presence of the promoter allows an alternative and more effective means for CO_2 activation which enables a bifunctional mechanism (Fig. 9) to exist where oxidation of the carbonaceous deposits located on the metallic surface takes place more efficiently by means of the oxygen species (likely hydroxyl groups) of the Ca-ZrLa support, that diffuse towards the metal particles (step 4). Therefore, formation of carbon deposits (step 1) was shown on this catalyst but to a limited extent as deduced from the experiment with the isotopic reaction mixture ($^{13}CH_4$–CO_2) where $CO/^{13}CO$ ratio was 1.2.

Reaction step 4 involves evolution of a second slower contribution to the hydrogen response which is limited by the formation and diffusion of the hydroxyl groups. Carbon dioxide reacts readily over the strongly basic CaO (step 2). The unbalance between the CO_2 reacted and the CO formed in TAP experiments and the carbonates species detected by DRIFTS confirms the existence of a pool of carbonates on Ni-Ca-ZrLa catalyst. The reverse of step 2 and step 3 account for the two contributions to the CO response with different rate of desorption that were identified in the isotopic TAP experiment.

The reaction steps proposed above are in agreement with the reaction mechanism reported for the dry reforming of methane performed at high temperature (873–973 K) [11] in spite that our study was performed at lower temperature (773 K) and that changes in the reaction mechanism with the temperature have been reported [17] and according to thermodynamic analysis would be expected [22]. Thus based on the individual CO_2 pulsing TAP experiments, CO disproportionation reaction is not considered, although thermodynamically favoured at the reaction temperature, as a via for deposition of deactivating carbon. These latter CO_2 pulsing TAP experiments evidence the maintenance of the CO_2 conversion and the CO production along the pulsing experiment over the two catalysts.

5. Conclusions

The specific features revealed by various transient kinetic experiments combined with DRIFTS permit a discrimination of the main elementary steps of methane and carbon dioxide activation and to get information about the origin of the formed carbon monoxide during the low temperature reforming of methane by carbon dioxide. Unlike the monofunctional mechanism proposed over Ni-ZrLa, a bifunctional mechanism is proposed over Ni-Ca-ZrLa to account for the presence of the promoter. The calcium oxide phase easily carbonated by CO_2 acts as a continuous supplier of gaseous CO and active oxygen species which react with the surface carbon arising from the methane cracking (the main route for the carbon deposit formation) on the nickel phase. The latter is assumed to hinder the formation of deactivating coke.

Acknowledgements

This work has been realized in the frame of the ACENET ERA-NET project METACOOR (ACE.07.012). Financial support by the MICINN of Spain (project CTQ2008-03068-E/PPQ) and the German Ministry of Education and Research (BMBF, contract no. 03X216) are gratefully acknowledged. The authors thank Dr. A. Barkschat for preparation of the catalysts.

Appendix A. Supplementary data

Supplementary data associated with this article can be found, in the online version, at http://dx.doi.org/10.1016/j.apcatb.2012.09.052.

References

[1] J.R. Rostrup-Nielsen, Catalysis Today 18 (1993) 305–324.
[2] S. Teuner, Hydrocarbon Processing 64 (1985) 106–107.
[3] A.M. Gadalla, B. Bower, Chemical Engineering Science 43 (1988) 3049–3062.
[4] J.A. Lercher, J.H. Bitter, W. Hally, W. Niessen, K. Seshan, Studies in Surface Science and Catalysis 101 (1996) 463–472.
[5] M.C.J. Bradford, M.A. Vannice, Applied Catalysis A 142 (1996) 73–96.
[6] J.A.C. Dias, J.M. Assaf, Catalysis Today 85 (2003) 59–68.
[7] Z. Boukha, M. Kacimi, M.F.R. Pereira, J.L. Faria, J.L. Figueiredo, M. Ziyad, Applied Catalysis A 317 (2007) 299–309.
[8] S.G. Liu, L.X. Guan, J.P. Li, N. Zhao, W. Wei, Y.H. Sun, Fuel 87 (2008) 2477–2481.
[9] M.-S. Fan, A.Z. Abdullah, S. Bhatia, ChemCatChem 1 (2009) 192–208.
[10] K. Sutthiumporn, S. Kawi, International Journal of Hydrogen Energy 36 (2011) 14435–14446.
[11] N.N. Sun, X. Wen, F. Wang, W.C. Peng, N. Zhao, F.K. Xiao, W. Wei, Y.H. Sun, J.T. Kang, Applied Surface Science 257 (2011) 9169–9176.
[12] P. Ferreira-Aparicio, I. Rodríguez-Ramos, A. Guerrero-Ruiz, Applied Catalysis A 237 (2002) 239–252.
[13] M.A. Soria, C. Mateos-Pedrero, A. Guerrero-Ruiz, I. Rodríguez-Ramos, International Journal of Hydrogen Energy 36 (2011) 15212–15220.
[14] J.R. Rostrup-Nielsen, J.-H. Bak Hansen, Journal of Catalysis 144 (1993) 38–49.
[15] X.E. Verykios, International Journal of Hydrogen Energy 28 (2003) 1045–1063.
[16] A. Olafsen, Å. Slagtern, I.M. Dahl, U. Olsbye, Y. Schuurman, C. Mirodatos, Journal of Catalysis 229 (2005) 163–175.
[17] Y.H. Cui, H.D. Zhang, H.Y. Xu, W.Z. Li, Applied Catalysis A 318 (2007) 79–88.
[18] S. Sokolov, E.V. Kondratenko, M.-M. Pohl, A. Barkschat, U. Rodemerck, Applied Catalysis B 113–114 (2011) 19–30.
[19] Y. Schuurman, C. Marquez-Alvarez, V.C.H. Kroll, C. Mirodatos, Catalysis Today 46 (1998) 185–192.
[20] A.N.J. van Keulen, K. Seshan, J.H.B. Hoenink, J.R.H. Ross, Journal of Catalysis 166 (1997) 306–314.
[21] J.T. Gleaves, G.S. Yablonskii, P. Phanawadee, Y. Schuurman, Applied Catalysis A 160 (1997) 55–88.
[22] M.K. Nikoo, N.A.S. Amin, Fuel Processing Technology 92 (2011) 678–691.
[23] R. Bouarab, O. Akdim, A. Auroux, O. Cherifi, C. Mirodatos, Applied Catalysis A 264 (2004) 161–168.
[24] Y.Q. Chen, Ch.W. Hu, M.Ch. Gong, X.H. Zhu, Y. Chen, A.M. Tian, Journal of Molecular Catalysis A 152 (2000) 237–244.
[25] E.M. Wilcox, G.W. Roberts, J.J. Spivey, Catalysis Today 88 (2003) 83–90.
[26] O. Demoulin, M. Navez, P. Ruiz, Catalysis Today 112 (2006) 153–156.
[27] D. Liu, G. Que, Z.X. Wang, Z.F. Yang, Catalysis Today 68 (2001) 155–160.
[28] C. Morterra, L. Orio, Materials Chemistry and Physics 24 (1990) 247–268.
[29] J.C. Lavalley, Catalysis Today 27 (1996) 377–401.
[30] J.A. Anderson, C.H. Rochester, Journal of the Chemical Society, Faraday Transactions I 82 (1986) 1911–1922.
[31] B. Bachiller-Baeza, I. Rodríguez-Ramos, A. Guerrero-Ruiz, Langmuir 14 (1998) 3556–3564.
[32] J.D.A. Bellido, J.E. De Souza, J.-C. de M'Peko, E.M. Assaf, Applied Catalysis 358 (2009) 215–223.

[33] N. Sun, X. Wen, F. Wang, W. Peng, N. Zhao, F. Xiao, W. Wei, Y. Sun, J. Kang, Applied Surface Science 257 (2011) 9169–9176.
[34] J.B. Peri, Journal of Catalysis 86 (1984) 84–94.
[35] C.W. Hu, Y.Q. Chen, P. Li, H. Min, Y. Chen, A. Tian, Journal of Molecular Catalysis A 110 (1996) 163–169.
[36] M.M.V.M. Souza, D.A.G. Aranda, M. Schmal, Journal of Catalysis 204 (2001) 498–511.
[37] A. Slagtern, Y. Schuurman, C. Leclercq, X. Verykios, C. Mirodatos, Journal of Catalysis 172 (1997) 118–126.
[38] A.M. Efstathiou, A. Kladi, V.A. Tsipouriari, X.E. Verykios, Journal of Catalysis 158 (1996) 64–75.
[39] A.M. O'Connor, Y. Schuurmanb, J.R.H. Ross, C. Mirodatos, Catalysis Today 115 (2006) 191–198.